G_nT motifs: short nucleotide tracts of ≥8bp that can increase T:A→G:C mutation rates >1000-fold in bacteria

Authors: James S. Horton[1,2], Joshua L. Cherry[3,4], Gretel Waugh[2], Tiffany B. Taylor[2]

Affiliations: [1]Institut Cochin, Université Paris Cité, INSERM U1016, CNRS UMR 8104, 75014 Paris, France. [2]Department of Life Sciences and Milner Centre for Evolution, University of Bath, Claverton Down, Bath, UK. [3]National Center for Biotechnology Information, National Library of Medicine, National Institutes of Health, Bethesda, Maryland, USA. [4]Division of International Epidemiology and Population Studies, Fogarty International Center, National Institutes of Health, Bethesda, Maryland, USA.

Author contributions: Experimental design by JSH. Experimental work by JSH and GW. Bioinformatics design and work by JLC. Data analysis by JSH and JLC. Manuscript written by JSH. Manuscript editing by all authors. JSH and GW were supervised and funded by TBT.

Keywords: Mutation hotspot, mutagenic nucleotide motif, local nucleotide context, homopolymeric tract, transversion mutation

Abstract:

Nucleotides across a genome do not mutate at equal frequencies. Instead, specific nucleotide positions can exhibit much higher mutation rates than the genomic average due to their immediate nucleotide neighbours. These 'mutational hotspots' can play a prominent role in adaptive evolution, yet we lack knowledge of which short nucleotide tracts drive hotspots. In this work, we employ a combinatorial approach of experimental evolution with *Pseudomonas fluorescens* and bioinformatic analysis of various *Salmonella* species to characterise a short nucleotide motif (≥8bp) that drives T:A→G:C mutation rates >1000-fold higher than the average T→G rate in bacteria. First, we experimentally show that homopolymeric tracts (≥3) of G with a 3' T frequently mutate so that the 3' T is replaced with a G, resulting in an extension of the guanine tract, i.e., GGGGT → GGGGG. We then demonstrate that the potency of this T:A→G:C hotspot is dependent on the nucleotides immediately flanking the G_nT motif. We find that the dinucleotide pair immediately 5' to a G_4 tract and the nucleotide immediately 3' to the T strongly affect the T:A→G:C mutation rate, which ranges from ~5-fold higher than the typical rate to >1000-fold higher depending on the flanking elements. Therefore the T:A→G:C hotspot motif is a product of several modular nucleotide components (1-4bp in length) which each exert a significant effect on the mutation rate of the G_nT motif. This work advances our ability to accurately identify the position and quantify the mutagenicity of hotspot motifs predicated on short tracts of nucleotides.

Introduction:

Mutation is the ultimate source of genetic variation that facilitates evolution. However, as most mutations are deleterious, species have evolved various prevention and repair mechanisms to decrease the average genomic mutation rate to very low frequencies. Bacterial species have some of the lowest average genomic mutation rates, which are typically around 10^{-10}-10^{-8} per nucleotide per generation (Lynch, 2010). However, while the average mutation rate may be very low, this is not true for all mutations. Instead, multiple biases skew the likelihood of observing particular mutations, driving some mutations to happen much more frequently than others. For example, transition bias (Stoltzfus and Norris, 2016) and A:T bias (Hershberg and Petrov, 2010) skew which nucleotide substitutions are more likely to occur, and deletion bias (Kuo and Ochman, 2009) skews DNA toward contraction rather than expansion. As well as biases in the types of mutations that are more common, certain genomic positions also exhibit higher mutation rates than others. For example, genomic macrodomains at intermediate positions exhibit higher mutation rates in multiple bacterial species (Dillon, Sung and Lynch, 2018), as do regions near sites of double-stranded breaks (Shee, Gibson and Rosenberg, 2012). More locally, promoter regions for genes facing away from the replication fork can exhibit an increase in indel rates (Sabari Sankar *et al.*, 2016). More locally still, a single nucleotide can have a mutation rate that is hundreds of times higher than a neighbouring nucleotide (Schroeder *et al.*, 2016). The primary determinant of this latter phenomenon is the local nucleotide sequence itself.

Local DNA sequence is the major driver of mutation rate heterogeneity throughout genomes, which is the case in both bacterial and in human DNA (Schroeder *et al.*, 2016; Liu and Samee, 2023). Nucleotide tracts of just five nucleotides can generate local spikes in mutation rate, commonly referred to as 'mutational hotspots'. These include recognition sequences for dcm methyltransferase (i.e. CCWGG), which increase C:G→T:A transition rate at the second C position by ~8-fold (Cherry, 2018). A more potent hotspot motif is a homopolymeric tract or simple sequence repeat (e.g. CCCCC). These are hotspots for indel mutations that cause the tract to either expand or contract by one or more nucleotides. A homopolymer of length five increases indel rates by ~100-fold, and the hotspot continues to increase in potency the longer the tract (Lee *et al.*, 2012). The transition rate of a nucleotide can also vary by ~400-fold depending on the single nucleotides situated either side of it (Schroeder *et al.*, 2016). Identifying which nucleotide sequences generate hotspots is therefore of central importance for predicting mutation rate heterogeneity throughout bacterial genomes. However, as not all nucleotide tracts that generate mutational hotspots are so readily identified, the challenge is to distinguish which nucleotide motifs impact local mutation rates.

76 In this work, we characterise a novel nucleotide motif that increases T:A→G:C mutation rates in
77 bacteria by up to a factor of ~1000 when on the leading replicative DNA strand. We show that
78 T:A→G:C substitution mutational hotspots are generated by a ≥7bp motif. The central
79 component of this motif is a homopolymeric tract of G immediately 5' to a T nucleotide. Similar
80 to indel hotspots, G tract length is strongly positively correlated with increased T:A→G:C
81 mutation rates at the T position when G length is ≥3. However, we also find that whether the
82 hereafter labelled G_nT tract operates as a potent mutational hotspot is determined by the
83 immediate flanking nucleotides. Rates of mutation are influenced by the 3' nucleotide following
84 the T and by the 5' dinucleotide immediately preceding the G tract, making these elements key
85 components of the G_nT motif. We demonstrate this hotspot motif through experiments with
86 *Pseudomonas fluorescens* complemented by bioinformatic analysis of *Salmonella* species. We
87 combine these data to show that the impact on mutation rate of each G_nT motif component is
88 similar in our two species. This suggests that the mutation rates for G_nT motifs determined for
89 this study will be good predictors of hotspot strength in other species of bacteria, particularly
90 *Gammaproteobacteria*.

91 Results:
92
93 *Homopolymeric tracts of guanine with a 3' thymine are primary components of T:A→G:C*
94 *mutational hotspots*
95
96 Recent analysis of numerous species from the NCBI Pathogens database has found that T:A→G:C
97 mutational hotspots in Pseudomonadota (Proteobacteria) and Bacillota (Firmicutes) are
98 generated when a T residue is preceded by tracts of G e.g., GGGGT→GGGGG (Cherry, 2023). The
99 potency of these hotspots increases with the length of the preceding guanine tract, with
100 T:A→G:C rates on average being over 400-fold higher when a T is preceded by 5 or more G's
101 relative to when it is preceded by 2 or fewer G's in *Salmonella*. This mutagenic effect is also much
102 more pronounced when the G_nT motif is on the leading strand of DNA replication (Cherry, 2023).
103
104 Prior to this finding, we performed experimental work using an immotile variant of *P. flourescens*
105 SBW25 and observed that, when populations of this bacterium re-evolved motility, this was most
106 often achieved by fixing mutations at a mutational hotspot within the gene *ntrB*. This hotspot,
107 A:T→C:G at position 289, was found to be sensitive to synonymous nucleotide variation, as the
108 introduction of six synonymous changes within 15bp of position 289 removed the hotspot in
109 SBW25 (Horton *et al.*, 2021). The local nucleotide context around the hotspot position was
110 therefore demonstrated to be integral to hotspot potency, but the components of the nucleotide
111 motif that drove the hotspot remained unknown.
112
113 The gene *ntrB* is natively encoded on the lagging strand, but from the perspective of the leading
114 strand during replication the hotspot nucleotide sequence 5'-3' is: GGGGT, which mutates to
115 become GGGGG. Therefore, this experimentally determined T:A→G:C mutational hotspot may
116 be an example of the phenomenon observed within the NCBI Pathogens dataset. The first
117 objective of the current study was to determine if guanine tract length was the primary facilitator
118 of the mutational hotspot within *ntrB*, and by doing so provide experimental evidence of the
119 widespread mutational hotspot phenomenon observed throughout many bacterial taxa.
120
121 Our approach for measuring changes in mutational hotspot potency was simple: we re-evolved
122 motility in immotile derivatives of *P. fluorescens* SBW25 and measured how often the hotspot
123 mutation was observed. The motility phenotype can be acquired through a single *de novo*
124 mutation from a pool of possible mutations in multiple loci, including the T:A→G:C mutation of
125 interest. We assessed hotspot potency by measuring the proportion of independent replicates
126 that acquired the T:A→G:C mutation as opposed to other viable mutations within the same gene
127 or elsewhere (Fig 1). If the proportion of independent replicates that acquired the T:A→G:C

hotspot mutation increased then this showed an increase in mutation rate at the motif, and if it decreased then the reverse was true.

For all but one strain, the only difference between the hotspot variants evolved for this study were 1-9 synonymous nucleotide variations within the gene *ntrB* that changed the local nucleotide sequence neighbouring the thymine position(s) of interest. Among the synonymous changes introduced were those that changed the length of the preceding G tract. We first pooled the results for all synonymous variant motifs surrounding a mutable T (explained in more detail in the next section) and looked at their hotspot potencies. We observed a clear positive correlation between T:A→G:C hotspot mutation rate and the length of the preceding G tract (Fig 1; R^2 = 0.82). Our dataset therefore experimentally corroborates the previous analysis in *Salmonella* and additionally demonstrates that the *ntrB* T:A→G:C hotspot is a product of the G_nT motif.

T:A→G:C hotspot motifs in experimental populations of P. fluorescens are contingent on preceding G tract length, the flanking 5' dinucleotide, and flanking 3' nucleotide

Having verified the importance of homopolymeric tracts of guanine for T:A→G:C mutational hotspots, we next asked whether the motif was affected by other nucleotides in the immediate neighbourhood. We assessed this question in two ways. Firstly, the coding sequence around the *ntrB* 289 hotspot has considerable codon flexibility, which allowed us to probe the impact of the immediate flanking nucleotides. We constructed strains with synonymous substitutions at the second position in the G tract (natively G_4T), the nucleotide 5' to the G tract, and the nucleotide 3' to the mutable T i.e. NGGNGTN (N = any nucleotide). Secondly, we wanted to confirm that any determined sequences exhibited high mutation rates only because of the short tract of nucleotides we augmented, and were not contingent on the wider nucleotide neighbourhood. To do this, we selected an alternative coding A:T position – 683 in *ntrB* – that had been previously shown to also facilitate motility (Horton *et al.*, 2021). This position natively has 3 preceding G's, which we were able to extend synonymously. Additionally, we were able to synonymously mutate the 5' dinucleotide i.e. SWNGGGTC (S = G/C, W = A/T). In total, we engineered and evolved 10 hotspot motif variants across the two hotspots positions in order to determine each nucleotide component's impact on hotspot potency (Fig 2).

Our results reveal that the modular components flanking the core of the hotspot motif – the 5' dinucleotide and the 3' nucleotide – exert a significant effect on the mutational hotspot. We evolved three variants of the 289 hotspot that had identical 5' TA dinucleotides and G tract lengths of 4 (G_4), with the only difference being the 3' nucleotide flanking the mutable T (Fig 2; bars 2-4). We observed that hotspot potency significantly decreased as the 3' nucleotide changed

from G to C to T (Fisher's exact test, p values < 0.0014). Similarly, two motifs around the 289 hotspot that only varied at the 5' nucleotide position (Fig 2; bars 3 and 5) revealed that a 5' A is significantly more mutable than a 5' C (Fisher's exact test, $p << 0.001$). Finally, two motifs with a 5' C, G_3 tract, and 3' C surrounding the 683 hotspot significantly differed in hotspot potency when the 5' dinucleotide partner changed from T to A (Fig 2, bars 7-8; Fisher's exact text, $p < 0.015$). The dinucleotide partner was also found to exert a significant effect on motifs of 5' A, G_4 tract, and 3' C around the 289 and 683 hotspots, as G was significantly more mutable than T (Fig 2, bars 3 and 10; $p < 0.001$).

These results show that the immediate flanking nucleotides are significant components of G_nT motifs. Additionally, our building of a hotspot at position 683 demonstrates that the motif is not contingent on the wider nucleotide neighbourhood. Outside of the 8bp motif window, the regions around positions 289 and 683 share very little sequence similarity (±6bp contains 2/12 base identity). Yet we were able to increase mutation rate at this position to surpass the native 289 position by augmenting only the established G_nT motif nucleotides. We observed that hotspot potency was significantly increased around position 683 when changing either the 5' dinucleotide partner or extending the G tract length to four (Fig 2, bars 7-9; Fisher's exact text, $p < 0.015$). The G_4 variant however remained significantly less mutable than the native 289 hotspot (Fig 2, bars 3 and 9; Fisher's exact text, $p < 0.01$) until we changed the 5' dinucleotide from CT to GA. After this change the 683 hotspot exceeded the native 289 hotspot sequence (Fig 2, bars 3 and 10; Fisher's exact text, $p << 0.001$). Therefore, by only augmenting the short nucleotide motif of 8-9bp (depending on G tract length) we are able to build T:A→G:C hotspots within multiple nucleotide neighbourhoods.

T:A→G:C hotspot motif analysis in natural populations of Salmonella shows that flanking nucleotides determine whether mutations rates are ~5-fold or >1000-fold above the genomic average

Our experimental assay with *Pseudomonas fluorescens* was able to demonstrate whether a nucleotide substitution within a T:A→G:C hotspot motif exerted a significant effect on hotspot potency. This assay is however limited, primarily by sample size, in its ability to reveal differences between hotspots with low mutation rates and sometimes between those with similar mutation rates. Another limitation is that we were only able to obtain rough estimates of relative mutation rates among motifs. Fortunately, we were able to reinforce our experimental data by re-analysing the *Salmonella* dataset that was generated by (Cherry, 2023) in order to accurately estimate the mutation rate for each unique G_nT motif. We adapted the original script from (Cherry, 2023) to estimate mutation rates for extended motifs that included the flanking nucleotides. As most of

203 our experimental data focussed on G_4T motifs we focus on this tract length for our analysis (Figs
204 3-4), but we also determined T:A→G:C mutation rates for G_3T and G_5T motifs (Sup figs 1-2).
205
206 Our analyses found that mutation rates differed by several orders of magnitude depending on
207 the flanking nucleotides. At the lowest end, flanking nucleotides of 5' AC and 3' A almost entirely
208 eliminate the G_4T motif hotspot, with T:A→G:C rates being only ~5.6-fold higher than genomic
209 T:A→G:C rates when there are no preceding G's (95% CI = 2.668-10.23; Fig 3). At the high end,
210 flanking nucleotides of 5' GA and 3' C lead to T:A→G:C mutation rates ~1112-fold higher than
211 the genomic average (95% CI = 1004-1185; Fig 3). In general, the mutation rate is highest when
212 the 3' nucleotide is a C, then G, then T, then A. For the 5' nucleotide the reverse is true, with
213 highest mutation rates being associated with A, then T, then C.
214
215 The 5' dinucleotide partner's influence is more variable and demonstrates the context-
216 dependency of motif mutagenicity. For example, 5' dinucleotide GA typically increases mutation
217 rates most, but TA is the most mutable when the 3' nucleotide is a G (Fig 3). This finding is
218 corroborated by our experimental data, as the mutation rate of 5' TA, 3' C is significantly lower
219 than both 5' TA, 3' G and 5' GA, 3' C (Fig 2, bars 2, 3 and 10). We additionally observed that the
220 relative impact of the flanking nucleotides on hotspot potency varies depending on G tract
221 length. For motifs with 3'C, the most mutable 5' dinucleotide is AA for G_3 (Sup fig 1), GA for G_4
222 (Fig 3), and CA or TA for G_5 (Sup fig 2). Similarly, for motifs with 5' TA, the most mutable 3'
223 nucleotides are C then G for G_3 (Sup fig 1), G then C for G_4 (Fig 4), and C then T for G_5 (Sup fig 2).
224
225 We next scrutinised the relationship between our datasets by comparing laboratory estimates of
226 relative mutation rates for various motifs in *P. fluorescens* to the estimates obtained for
227 *Salmonella* from analysis of natural isolates (Fig 4). The relative rates correlate well between the
228 two organisms (Spearman's rank order correlation, rho = 0.94, $p < 0.02$). This correlation
229 coefficient is expected to be an underestimate due to uncertainty in the rate estimates, especially
230 the large uncertainties observed for our *P. fluorescens* data. Despite this, the two datasets
231 exhibited highly similar mutation rate estimates for the set of motifs we analysed.
232
233 The *Salmonella* analyses reinforce the finding that the flanking nucleotides are important
234 determinants of mutation rates at G_nT motifs, and the data provide accurate quantifications of
235 the flanking nucleotide impact on mutation rates. The analyses also show that the effects of the
236 5' dinucleotide, G tract length, and 3' nucleotide on T:A→G:C mutation rate are not independent.
237 Rather, the effect on mutation rate of changing one component of the motif is contingent on the
238 other components.

239 Discussion:
240
241 Mutation rates across a genome are shaped by multifaceted mechanisms, resulting in significant
242 variation rather than uniformity. Specific sites, known as 'mutational hotspots,' exhibit mutation
243 rates much higher than the genomic average and can influence both the direction and
244 predictability of bacterial adaptation (Horton and Taylor, 2023). While it's known that local
245 nucleotide sequences impact mutation rates (Schroeder *et al.*, 2016), the specific features and
246 combinations defining hotspots are not well understood. In this study, we employed
247 experimental and bioinformatic methods to characterise a short nucleotide motif (G_nT) that can
248 increase T:A→G:C mutation rates by over 1000-fold in bacteria. Through experimental evolution
249 with *P. fluorescens* and complementary bioinformatic analysis of *Salmonella* species, we build on
250 previous work that found that T:A→G:C mutation hotspots are generated by homopolymer G
251 tracts with a 3' T (Cherry, 2023) to show that G_nT motifs depend on homopolymeric G tracts in
252 combination with the flanking nucleotides. These findings highlight the modularity of hotspot
253 components, providing insights that could enhance predictive models of mutation rate
254 variability.
255
256 *Possible mechanism*
257
258 The mechanism driving high mutation rates at G_nT motifs is unclear. However, the central role
259 played by the homopolymeric tract (also referred to as a simple sequence repeat) suggests
260 slipped-strand mispairing as a causal factor. During DNA replication, dissociated parent and
261 nascent DNA strands can re-anneal out of register due to homology with other nucleotides in the
262 repeat region (Levinson and Gutman, 1987). This process typically results in an indel mutation as
263 the out-of-register mispairing causes a nucleotide to loop out of either the nascent or template
264 strand, causing an insertion or deletion of the repetitive nucleotide respectively (Fan and Chu,
265 2007). In this study we observe a substitution mutation, but this may be a product of slipped-
266 strand mispairing if the T→G mutation is caused by insertion of a G followed by another
267 dissasociation event and re-pairing in the original register, resulting in a G:A mispair. If extension
268 then continues and the mismatch is not repaired, the result will be a substitution of the original
269 T:A hotspot position with its replacement G:C.
270
271 It is not clear how the flanking nucleotides contribute to the proposed slipped-strand events,
272 although there are several possibilities. Short nucleotide sequences that generate mutational
273 hotspots during DNA replication must overcome multiple barriers. A sequence must initially
274 exploit error-prone features of the replicating polymerase to generate a mismatch or indel, and
275 subsequently this error must evade proof-reading and mismatch repair to ensure that the
276 mutation becomes immortalised. The flanking nucleotides may contribute to mutagenicity during

this process, either by facilitating the slipped-strand mispairing events - by making the DNA sequence more prone to opening or "breathing" (Oron-Karni *et al.*, 1997; Jose *et al.*, 2009) - or by aiding the resultant error to remain unrecognised by DNA proofreading and repair enzymes.

Proofreading by DNA polymerase discriminates mismatches by checking for correct Watson-Crick geometry (Bębenek and Ziuzia-Graczyk, 2018), likewise mismatch repair recognises errors based on DNA secondary structure (Pavlova *et al.*, 2020). Previous works have found direct and indirect evidence that immediate flanking nucleotides can help stabilise mismatches (Allawi and SantaLucia, 1998; Long *et al.*, 2018), and that the structure of the DNA helix can be impacted several nucleotides away from a mismatch (Rossetti *et al.*, 2015). We estimated melting temperatures for all 48 G_4T motif sequences assuming a G:A mismatch and when we controlled for the 5' nucleotide we found a significant positive correlation between DNA stability and mutation rate for the 5' dinucleotide partner and 3' nucleotide. Conversely, when we controlled for the 3' nucleotide we observed a mostly non-significant but negative correlation between stability and mutation rate for the 5' nucleotide and 5' dinucleotide partner (Sup fig 3). This relationship can be explained by the preference for C:G/G:C at the 3' position and against C:G/G:C at the 5' position. Therefore the flanking nucleotides may impact the stability in different ways, e.g. the low stability of the 5' dinucleotide may facilitate DNA dissasociation and breathing, while the 3' nucleotide may stabilise the DNA double helix following a return to an in-register mismatch, helping the error to evade repair. If DNA stability is an important factor in hotspot potency, we can speculate further and note that the purine-purine G•A pair exhibits unique undertwisting of the DNA helix relative to other mismatches (Rossetti *et al.*, 2015), which may help explain why the homopolymer substitution phenomenon appears to be unique to G_nT motifs (Cherry, 2023). Finally, while documentations of sequential indel and mismatch events resulting from strand-slippage are rare, at least one study has previously reported on the phenomenon and implicated DNA breathing in facilitating the effect (Oron-Karni *et al.*, 1997).

Quantifying and controlling mutagenesis

A key advantage to identifying the modular nucleotide components of hotspot motifs and quantifying their impact on hotspot strength is that it allows us to accurately predict mutation rates. It is reassuring that the relative mutation rates of G_nT motifs determined from *Salmonella* are applicable to *P. fluorescens*, a distantly related species in the *Gammaproteobacteria* class (Williams et al., 2010). This suggests that predicting mutation rates at G_nT hotspot motifs using the *Salmonella* data will be reasonably accurate across broad genomic backgrounds. However, the potencies of hotspot motifs are additionally influenced by other genomic features such as genomic position and DNA structure (Shepherd, Horton and Taylor, 2022; Liu and Samee, 2023). Thus, it is less certain whether identical motifs within the same genome mutate at the same rates.

The previous *Salmonella* analysis examined rates of T:A→G:C accumulation at G_nT motifs as a function of chromosome position and found a roughly uniform distribution (Cherry,2023). This suggests that there is no strong systematic dependence of hotspot potency on genome position. However, our previous work found that the *ntrB* G_nT motif is more potent when situated in its native position as opposed to the Tn7 insertion site, which is situated on the other replichore and is closer to the replication origin (Shepherd et al., 2022). Additionally, recent work has shown that DNA replication error hotspots are affected by multiple genomic properties that fluctuate throughout the genome (Hasenauer *et al.*, 2024). Therefore, there may be instances where hotspot potency changes by perhaps an order of magnitude (using the data from Shepherd et al., 2022, as a rough guide) depending on genomic context. However, this phenomenon does not appear to be a simple effect of distance from the origin of replication.

The external genomic parameters influencing the exact mutagenicity of G_nT motifs are yet to be determined, but our combinatorial data show that the local eight-base pair nucleotide motif is the major determinant of T:A→G:C hotspot mutation rate throughout, and across, bacterial genomes. Therefore, finding these motifs in sequence data can identify the location of potent T:A→G:C hotspots. For example, there are 2078 naturally occuring $G_{3\text{-}5}T$ motifs on the leading replicative strand of *P. fluorescens* SBW25 with forecast mutation rates >100-fold above the genomic average. Of these, ≥1206 genes (~20% of reading frames) posess at least one hotspot motif that would result in a non-synonymous T:A→G:C substitution. As well as occurring naturally in many coding sequences, G_nT motifs are so short that they can also be readily engineered into circuits to help control the evolvability of a system. We investigated this with an experiment where we added two hotspot motifs into the *ntrB* gene, and predictably observed that evolution happened significantly faster and became more predictable at the level of locus (Sup fig 4). There is a growing interest in our ability to both forecast and exert control over the evolutionary process (Lind *et al.*, 2019; Castle, Grierson and Gorochowski, 2021). G_nT motifs, as agents that heavily bias the process of mutation, have the potential to contribute to both of these goals.

342 Methods:
343
344 *Strains and culture conditions*
345
346 Experiments were performed using populations derived from *Pseudomonas fluorescens* SBW25
347 strain AR2 (SBW25ΔfleQ IS-ΩKm-hah: PFLU2552) which lacks functionality of FleQ and ViscB,
348 rendering populations immotile (Alsohim *et al.*, 2014). The strains constructed from this genomic
349 background contain synonymous nucleotide substitutions in the gene *ntrB*, which has previously
350 been found to resurrect motility under directional selection following a one-step *de novo*
351 mutation in the coding sequence. *P. fluorescens* populations were cryogenically stored at -70°C
352 and grown at 27°C; overnight cultures were agitated at 180rpm. *E. coli* strains used for cloning
353 (DH5α), conjugal transfer (SP50 pRK2073), transposon-mediated genome incorporation (S17
354 pTNS2), and allelic exchange (ST18) were cryogenically stored at -70°C and grown at 37°C;
355 overnight cultures were agitated at 200rpm.
356
357 Antibiotics used in this study were prepared at the following working concentrations: 50 µg/ml
358 kanamycin sulfate; 100 µg/ml ampicillin sodium salt; 30 µg/ml gentamicin sulfate; 10 µg/ml
359 tetracycline hydrochloride; 250 µg/ml streptomycin sulfate salt. All antibiotics were purchased
360 from Sigma-Aldrich.
361
362 *Synonymous manipulations of ntrB*
363
364 To generate synonymous motif variants, we amplified the *ntrBC* operon from *P. fluorescens*
365 SBW25 derivatives (NCBI Assembly: ASM922v1, GenBank sequence: AM181176.4) using outside
366 primers ntrBC-HindIII-F and ntrBC-SacI-R (Sup Table 1). In the first PCR, we generated two
367 fragments using the outside primers in combination with complementary oligonucleotides that
368 had approximately 40bp homology to the nucleotide tract flanking *ntrB* position 289 or 683,
369 depending on the desired construct (Sup Table 1). In the second PCR, we annealed these two
370 fragments with complementary overhangs to generate a complete *ntrBC* operon with
371 synonymous variations at positions neighbouring 289 or 683. For *ntrB* 289 variants we used *P.*
372 *fluorescens* SBW25 strain AR2 as template DNA; for *ntrB* 683 variants we used *P. fluorescens*
373 SBW25 strain AR2-sm as template DNA to remove the native hotspot at *ntrB* 289. All changes
374 made to the nucleotide sequence left the encoded protein sequence unchanged, both with the
375 original T and with the G resulting from the mutations of interest. Most were single-base changes
376 at third positions of codons. The exception was a change of AGC, which encodes serine, to TCC,
377 which also encodes serine.
378
379 *Genomic integration of variant sequences through mini-Tn7 mediated transposition*

380

381 All *ntrBC* operon variants, aside from 289-TAGGCGTC, were integrated into a non-motile *P.*
382 *fluorescens* SBW25 derivative AR2 Δ*ntrBC* genomic background using mini-Tn7 mediated
383 transposition (Choi and Schweizer, 2006). As the native operon has been deleted in the host
384 genomic background this incorporation operates as a functional translocation. Generated *ntrBC*
385 inserts and the plasmid pJM220 (pUC18T-miniTn7T-gm-rhaSR-PrhaBAD; a gift from Joanna
386 Goldberg (http://n2t.net/addgene:110559; RRID:Addgene_110559); see Meisner and Goldberg,
387 2016) were digested with the restriction enzymes HindIII-HF and SacI-HF (NEB) for 1h at 37°C.
388 This was followed by a 30-minute digestion at 37°C where RSAP (NEB) was added to the pJM220
389 digestion mix. The vector and insert were gel-extracted and purified with a Monarch® DNA gel
390 extraction kit (NEB) and the fragments were annealed using T4 DNA ligase (NEB) ligation at 16°C
391 for 12h, followed by 4°C hold for ~4h. The ligated plasmid was transformed into cloning *E. coli*
392 strain DH5α and plated onto LB agar containing ampicillin and gentamicin. Conjugal transfer was
393 performed by preparing 10ml overnight LB broth cultures of the recipient *P. fluorescens* strain
394 (supplemented with kanamycin), DH5α pJM220-*ntrBC* (supplemented with ampicillin and
395 gentamicin), and the helper plasmids SP50 pRK2073 (supplemented with streptomycin) and S17
396 pTNS2 (supplemented with ampicillin). 700µl of the *P. fluorescens* culture was combined with
397 100µl of each *E. coli* strain to produce 1ml final volume. The mixed population was pelleted
398 through centrifugation at 8000 rcf for 3 minutes, the supernatant removed, and re-suspended in
399 1ml fresh LB broth. This process was repeated two additional times to remove residual antibiotic
400 in the culture, before a final re-suspension in 50µl LB broth. This mixed culture was added in a
401 puddle to an LB agar plate containing no antibiotic and left for ~20-30 minutes in a laminar flow
402 hood to dry. The puddle was incubated at 27°C for a minimum of 5h before an inoculating loop
403 was used to transfer a streak from the centre of the puddle to fresh LB agar supplemented with
404 kanamycin and gentamicin. This plate was incubated at 27°C for 1-2 days until distinct colonies
405 could be observed. Cryogenic clonal stocks were produced by growing one colony overnight at
406 27°C in the presence of kanamycin and gentamicin and storing the resultant culture in 20%
407 glycerol final volume at -70°C.
408

409 *Scarless synonymous augmentation of ntrB through two-step allelic exchange*
410

411 Synonymous variant 289-TAGGCGTC, which is identical to progenitor strain AR2 except for a C→G
412 at nucleotide 291 on the coding strand of the gene *ntrB*, was created through two-step allelic
413 exchange. This protocol closely followed that outlined by (Hmelo *et al.*, 2015), barring
414 amendments outlined in (Horton *et al.*, 2021), which were made to optimise the protocol for
415 *Pseudomonas fluorescens*. Primers utilised for this work are outlined in Sup Table 1. In brief, an
416 augmented *ntrB* sequence was produced through two PCR steps as outlined above using AR2 as
417 template data, with the amendment that nested primers ntrB_np_F and ntrB_np_R were used

418 to combine the two fragments and add restriction enzyme recognition sequences in the second
419 PCR. The produced insert, and the vector pTS1, were digested with restriction enzymes BamHI-
420 HF and Hind-III-HF (NEB), gel extracted, and ligated as described above. The ligated plasmid was
421 then transformed into *E. coli* strain ST18 and plated onto LB agar supplemented with 50 µg/ml 5-
422 aminolevulinic acid. The transformed ST18 strain was conjugated with *P. fluorescens* SBW25
423 derivative AR2 by mixing 750 µl ST18 with 250 µl AR2 and pelleting and puddle mating as outlined
424 above. The conjugative puddle was left to incubate overnight on LB agar supplemented with 50
425 µg/ml 5-aminolevulinic acid, and a streak was transferred onto LB agar supplemented with
426 tetracycline to select for merodiploid AR2 strains. Two-step recombinants were then selected for
427 by plating on NSLB agar containing +15% w/v sucrose, which selects against merodiploids.
428 Surviving colonies were either *ntrB* C291G mutants or revertants to the AR2 progenitor genotype.
429 Successful mutants were verified by Sanger sequencing of the *ntrB* locus using ntrB_1119_F and
430 ntrB_1119F_R. Cryogenic stocks were then prepared as detailed above.
431
432 *Experimental evolution to assess hotspot potency*
433
434 We used soft agar motility assays to select for mutations that restore motility, including the
435 T:A→G:C mutations at positions 289 and 683 in *ntrB* (from Taylor *et al.*, 2015). To prepare soft
436 agar, we poured 30 ml of molten LB broth (Sigma-Aldrich) containing 0.25% agar (Fisher
437 Scientific) into standard 88 mm diameter petri dishes and left these overnight to solidify. The
438 following morning, the petri dishes were placed in a laminar flow hood with the lids removed for
439 30 minutes to dry. A sterile cocktail stick was then used to transfer a single colony to the soft
440 agar. The stick was held perpendicular to the agar and the colony inserted ~2 mm. Plates were
441 inoculated in the centre of the dish aside from strains 289-TCGGGGTC, 289-TAGGCGTC, and 683-
442 TCGGGTC, which were inoculated with four equally separated colonies. The plates were
443 incubated at 27°C and monitored daily for emergence of motility zones for ≤12 days. The first
444 motile zone to appear per plate was passaged onto fresh agar containing kanamycin and
445 gentamicin by inserting an inoculating loop into the leading edge of the motile zone and streaking
446 to produce single colony forming units. The motility plate was then discarded to ensure that all
447 emergent motile populations evolved independently.
448
449 Passaged plates were incubated for 48 h at 27°C and a single colony was used as template DNA
450 for a colony PCR with primers ntrB_1119_F and ntrB_1119_R (Sup Table 1). The generated *ntrB*
451 amplicons were purified using a Monarch® PCR DNA clean-up kit (NEB) and Sanger sequencing
452 was performed by Source Bioscience using ntrB_1119_F as a primer. *ntrB* reads provided by
453 Source Bioscience were manually trimmed to remove ~50bp from each terminus to remove
454 substitution and 1bp indel calls of low confidence. Mutations of high confidence were called by

aligning the *ntrB* sequence against the SBW25 reference genomic sequence (NCBI Assembly: ASM922v1, GenBank sequence: AM181176.4) using BLAST.

Analysis of hotspot motifs in Salmonella species

Estimation of relative mutation rates in natural populations of *Salmonella* was based on the data from Cherry (2023). The number of T→G mutations inferred to have occurred in a sequence context of interest was divided by the number of such sites per genome (a weighted average among many *Salmonella* genomes, as detailed in Cherry (2023)). Confidence intervals were calculated assuming a Poisson sampling distribution for the number of mutations.

Statistical analysis

Statistical analyses were performed using R version 4.4.1 (2024-06-14). For experimental data, changes in hotspot potency were determined using Fisher's exact test (fisher.test, from the stats package exact2x2, v4.4.0) with $p < 0.05$ treated as significant. Fold-changes in potency were calculated using Fisher's exact test's odds ratio alongside the produced 95% confidence intervals. Figures were generated using R's *ggplot* package v3.5.1. DNA stability with a G:A mismatch at the mutable T positions was estimated using the R package *rmelting* v1.20.0 (Aravind and Krishna, 2024) with the following parameters: nucleic acid concentration = 2×10^{-6}, Na concentration = 1.

Funding:

This project was supported by a BBSRC NI grant (BB/T012994/1; awarded to T.B.T.) supporting J.S.H. and G.W., and a Royal Society Dorothy Hodgkin Research Fellowship (DH150169) awarded to and supporting T.B.T. This work was supported in part by the Division of Intramural Research (DIR) of the National Library of Medicine (NLM), National Institutes of Health. The opinions expressed in this article are those of the author and do not reflect the view of the National Institutes of Health, the Department of Health and Human Services, or the US government.

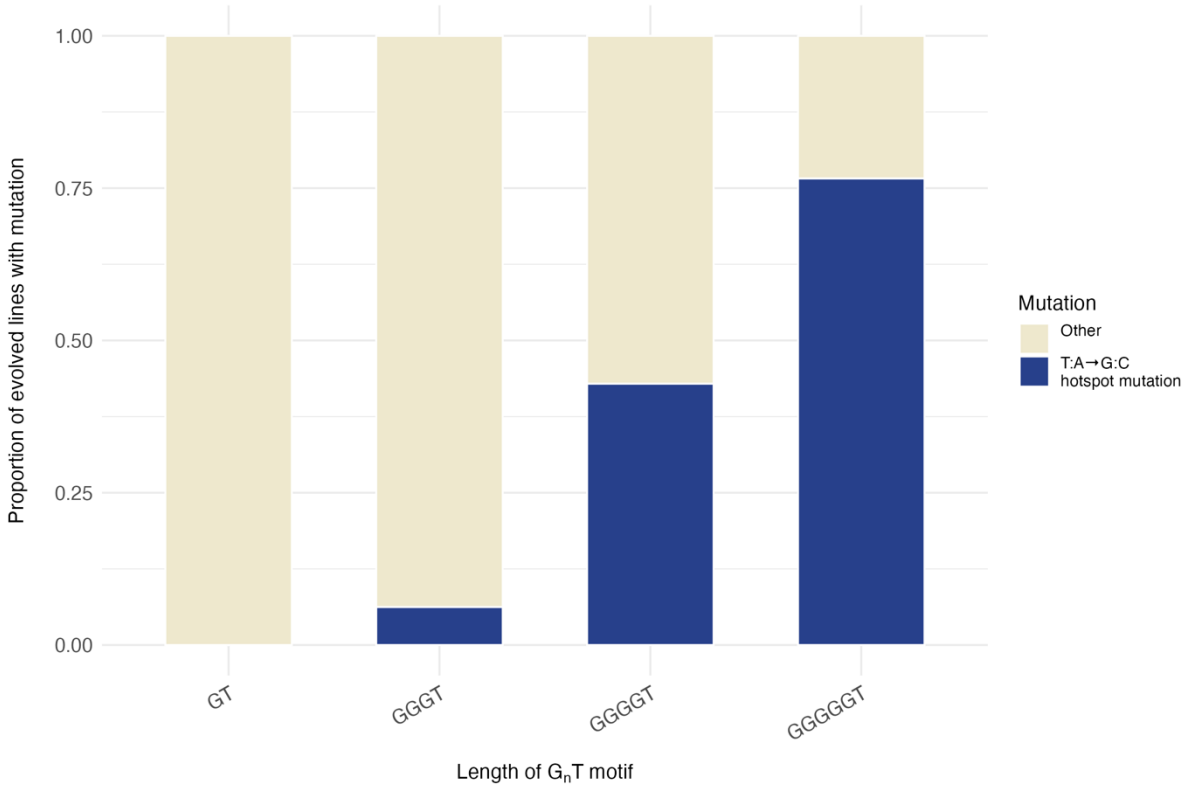

484 **Fig 1. T:A→G:C mutation frequency is positively correlated with length of the preceding G tract.**
485 10 *ntrB* variants with synonymous nucleotide changes neighbouring a T position were used to
486 study the T:A→G:C hotspot motif. Each motif variant contained a homopolymeric tract of
487 guanine 5' to the T that was either 1, 3, 4, or 5 bp in length. Shown are the aggregated proportion
488 of evolved mutant lines that acquired a T:A→G:C hotspot mutation when the thymine of interest
489 is preceded by 1 G (one strain, *n* = 29), 3 G's (two strains, *n* = 112), 4 G's (six strains, *n* = 434), or
490 5 G's (one strain, *n* = 47). Total evolved replicates = 622. Overall our experimental work finds that
491 preceding G tract length is a strong determinant of a T:A→G:C mutational hotspot (R^2 = 0.82).

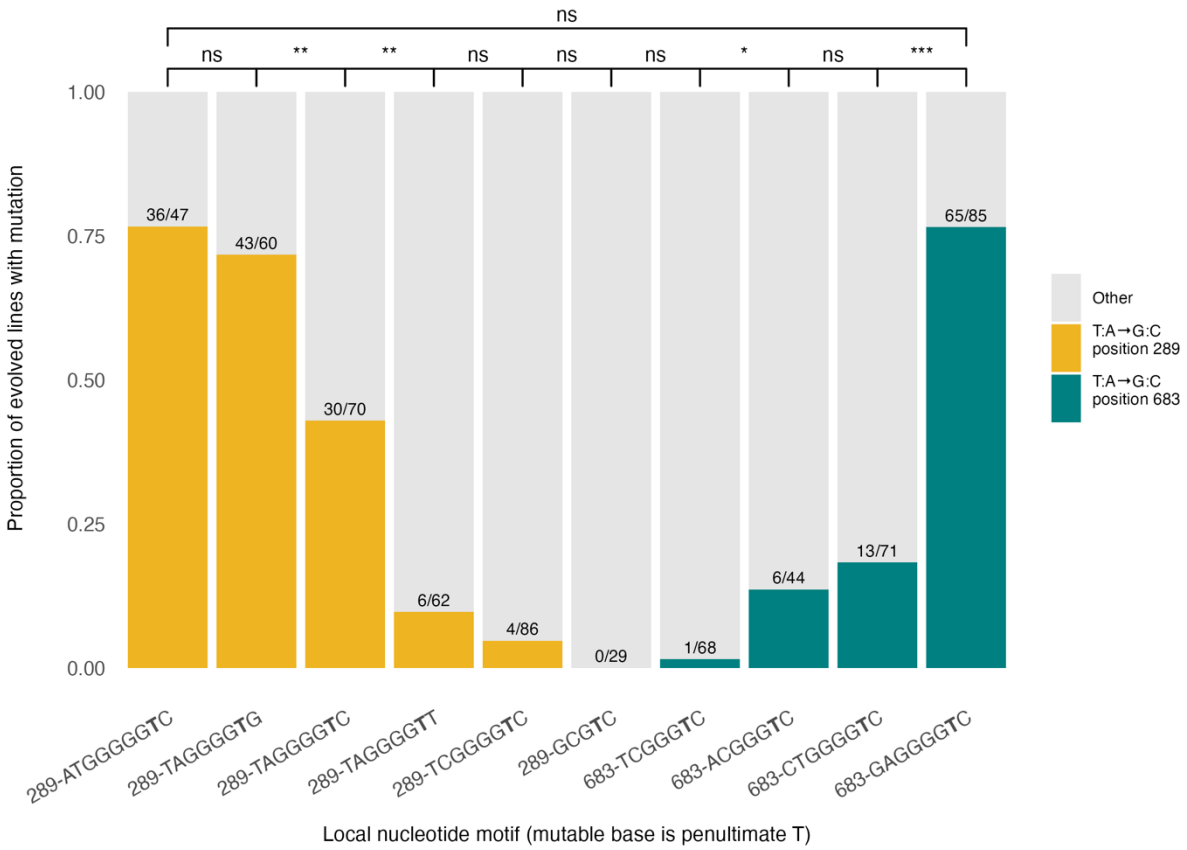

Fig 2. The frequency of T:A→G:C mutation in *P. fluorescens* is strongly influenced by neighbouring G tract length and flanking nucleotide sequence. Mutation frequencies of T:A→G:C are shown for a suite of short synonymous nucleotide tract variants surrounding two T positions within the gene *ntrB*. The sequences on the x-axis, listed 5'-3' with respect to leading strand replication, show the elements observed to influence mutation rate: the dinucleotide 5' to the guanine tract, a homopolymeric tract of guanine (1-5bp in length), the hotspot T position that mutates into G (bold), and the nucleotide 3' to the mutable thymine. T:A→G:C hotspot motifs were augmented around two thymine positions in *ntrB*: coding position 289 (yellow bars) and coding position 683 (teal bars). The y axis shows the proportion of independent populations that acquired the T:A→G:C hotspot mutation, calculated from the observed counts plotted over each bar. Significance values were determined using Fisher's exact test (* $p < 0.05$; ** $p < 0.01$; *** $p < 0.001$).

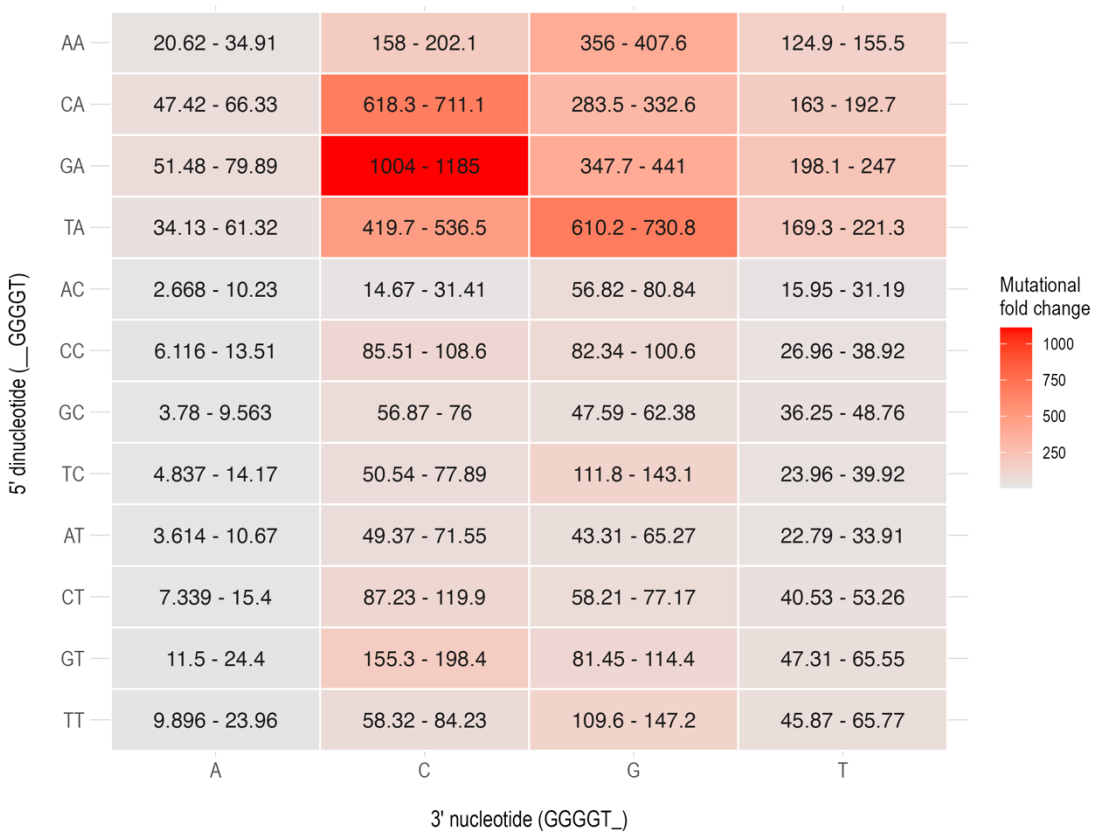

Fig 3. The impact of flanking nucleotides neighbouring G_4T tracts on T:A→G:C mutation rates in natural *Salmonella* populations. A heatmap showing the T:A→G:C mutation rate for G_4T motif variants relative to the average T:A→G:C genomic mutation rate with no preceding Gs. Each panel represents a unique combination of nucleotides (5' dinucleotide on y axis and 3' nucleotide on x axis) flanking a G_4T motif**.** Panels are coloured according to mean mutation rate and annotated with 95% confidence intervals.

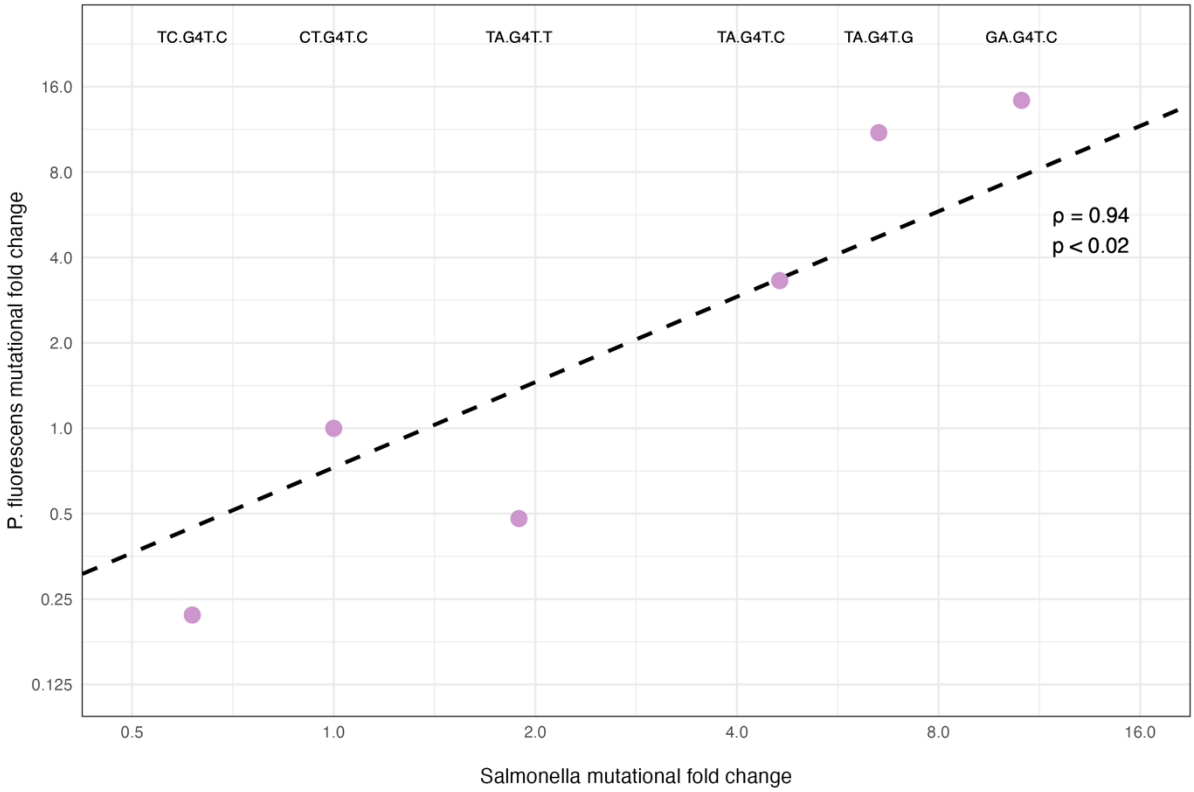

Fig 4. Relative mutation rates of G_4T motifs in *P. fluorescens* are highly predictive of those in *Salmonella*. An experimental P. *fluorescens* dataset and analysis of natural *Salmonella* populations were made comparable by determining mutational fold-changes of G_4T motifs (labels) relative to the motif CTG_4TC (CT.G4T.C). Points show mutational fold changes of *P. fluorescens* motifs (y-axis; determined by Fisher's exact test odds ratio) and fold changes observed for each motif in *Salmonella* (x-axis; see Methods). The line represents the least squares fit in the log domain. Values for rho and *p* were determined by a Spearman rank-order correlation.

518 References:

519

520 Allawi, H.T. and SantaLucia, J. (1998) 'Nearest-neighbor thermodynamics of internal A.C
521 mismatches in DNA: sequence dependence and pH effects', *Biochemistry*, 37(26), pp. 9435–
522 9444. Available at: https://doi.org/10.1021/bi9803729.

523 Alsohim, A.S. *et al.* (2014) 'The biosurfactant viscosin produced by Pseudomonas fluorescens
524 SBW25 aids spreading motility and plant growth promotion', *environmental microbiology*,
525 16(7), pp. 2267–2281.

526 Aravind, J. and Krishna, G. (2024) 'rmelting: R Interface to MELTING 5'. Available at:
527 https://aravind-j.github.io/rmelting/.

528 Bębenek, A. and Ziuzia-Graczyk, I. (2018) 'Fidelity of DNA replication-a matter of proofreading',
529 *Current Genetics*, 64(5), pp. 985–996. Available at: https://doi.org/10.1007/s00294-018-0820-1.

530 Castle, S.D., Grierson, C.S. and Gorochowski, T.E. (2021) 'Towards an engineering theory of
531 evolution', *Nature Communications*, 12(1), p. 3326. Available at:
532 https://doi.org/10.1038/s41467-021-23573-3.

533 Cherry, J.L. (2018) 'Methylation-Induced Hypermutation in Natural Populations of Bacteria',
534 *Journal of Bacteriology*, 200(24), pp. e00371-18.

535 Cherry, J.L. (2023) 'T Residues Preceded by Runs of G Are Hotspots of T→G Mutation in
536 Bacteria', *Genome Biology and Evolution*, 15(6), p. evad087. Available at:
537 https://doi.org/10.1093/gbe/evad087.

538 Choi, K.H. and Schweizer, H.P. (2006) 'mini-Tn7 insertion in bacteria with single attTn7 sites:
539 Example Pseudomonas aeruginosa', *Nature Protocols*, 1(1), pp. 153–161. Available at:
540 https://doi.org/10.1038/nprot.2006.24.

541 Dillon, M.M., Sung, W. and Lynch, M. (2018) 'Periodic Variation of Mutation Rates in Bacterial
542 Genomes', *mBio*, 9(4), pp. 1–15.

543 Fan, H. and Chu, J.-Y. (2007) 'A Brief Review of Short Tandem Repeat Mutation', *Genomics,*
544 *Proteomics & Bioinformatics*, 5(1), pp. 7–14. Available at: https://doi.org/10.1016/S1672-
545 0229(07)60009-6.

546 Hasenauer, F.C. *et al.* (2024) 'Genome-wide mapping of spontaneous DNA replication error-
547 hotspots using mismatch repair proteins in rapidly proliferating Escherichia coli', *Nucleic Acids*
548 *Research* [Preprint]. Available at: https://doi.org/10.1093/nar/gkae1196.

549 Hershberg, R. and Petrov, D.A. (2010) 'Evidence That Mutation Is Universally Biased towards AT
550 in Bacteria', *PLOS Genetics*, 6(9), p. e1001115. Available at:
551 https://doi.org/10.1371/journal.pgen.1001115.

552 Hmelo, L.R. *et al.* (2015) 'Precision-engineering the Pseudomonas aeruginosa genome with two-
553 step allelic exchange', *Nature Protocols*, 10(11), pp. 1820–1841. Available at:
554 https://doi.org/10.1038/nprot.2015.115.

555 Horton, J.S. *et al.* (2021) 'A mutational hotspot that determines highly repeatable evolution can
556 be built and broken by silent genetic changes', *Nature Communications*, 12(6092), pp. 1–10.
557 Available at: https://doi.org/10.1038/s41467-021-26286-9.

558 Horton, J.S. and Taylor, T.B. (2023) 'Mutation bias and adaptation in bacteria', *Microbiology*,
559 169(11), p. 001404. Available at: https://doi.org/10.1099/mic.0.001404.

560 Jose, D. *et al.* (2009) 'Spectroscopic studies of position-specific DNA "breathing" fluctuations at
561 replication forks and primer-template junctions', *Proceedings of the National Academy of*
562 *Sciences*, 106(11), pp. 4231–4236. Available at: https://doi.org/10.1073/pnas.0900803106.

563 Kuo, C.-H. and Ochman, H. (2009) 'Deletional Bias across the Three Domains of Life', *Genome*
564 *Biology and Evolution*, 1, p. 145. Available at: https://doi.org/10.1093/gbe/evp016.

565 Lee, H. *et al.* (2012) 'Rate and molecular spectrum of spontaneous mutations in the bacterium
566 Escherichia coli as determined by whole-genome sequencing', 109(41). Available at:
567 https://doi.org/10.1073/pnas.1210309109/-
568 /DCSupplemental.www.pnas.org/cgi/doi/10.1073/pnas.1210309109.

569 Levinson, G. and Gutman, G.A. (1987) 'Slipped-strand mispairing: a major mechanism for DNA
570 sequence evolution', *Molecular Biology and Evolution*, 4(3), pp. 203–221. Available at:
571 https://doi.org/10.1093/oxfordjournals.molbev.a040442.

572 Lind, P.A. *et al.* (2019) 'Predicting mutational routes to new adaptive phenotypes', *eLife*, 8, p.
573 e38822. Available at: https://doi.org/10.7554/eLife.38822.

574 Liu, Z. and Samee, M.A.H. (2023) 'Structural underpinnings of mutation rate variations in the
575 human genome', *Nucleic Acids Research*, 51(14), pp. 7184–7197. Available at:
576 https://doi.org/10.1093/nar/gkad551.

577 Long, H. *et al.* (2018) 'Specificity of the DNA Mismatch Repair System (MMR) and Mutagenesis
578 Bias in Bacteria', *Molecular Biology and Evolution*, 35(10), pp. 2414–2421. Available at:
579 https://doi.org/10.1093/molbev/msy134.

580 Lynch, M. (2010) 'Evolution of the mutation rate', *Trends in genetics : TIG*, 26(8), pp. 345–352.
581 Available at: https://doi.org/10.1016/j.tig.2010.05.003.

582 Meisner, J. and Goldberg, J.B. (2016) 'The Escherichia coli rhaSR-PrhaBAD inducible promoter
583 system allows tightly controlled gene expression over a wide range in Pseudomonas
584 aeruginosa', *Applied and Environmental Microbiology*, 82(22), pp. 6715–6727. Available at:
585 https://doi.org/10.1128/AEM.02041-16.

586 Oron-Karni, V. *et al.* (1997) 'A Novel Mechanism Generating Short Deletion/Insertions Following
587 Slippage is Suggested by a Mutation in the Human α2-Globin Gene', *Human Molecular Genetics*,
588 6(6), pp. 881–885. Available at: https://doi.org/10.1093/hmg/6.6.881.

589 Pavlova, A.V. *et al.* (2020) 'Responses of DNA Mismatch Repair Proteins to a Stable G-
590 Quadruplex Embedded into a DNA Duplex Structure', *International Journal of Molecular*
591 *Sciences*, 21(22), p. 8773. Available at: https://doi.org/10.3390/ijms21228773.

592 Rossetti, G. *et al.* (2015) 'The structural impact of DNA mismatches', *Nucleic Acids Research*,
593 43(8), pp. 4309–4321. Available at: https://doi.org/10.1093/nar/gkv254.

594 Sabari Sankar, T. *et al.* (2016) 'The Nature of Mutations Induced by Replication-Transcription
595 Collisions', *Nature*, 535(7610), pp. 171–181. Available at:
596 https://doi.org/10.1016/j.physbeh.2017.03.040.

597 Schroeder, J.W. *et al.* (2016) 'The effect of local sequence context on mutational bias of leading
598 and lagging strand genes', *Current Biology*, 26(5), pp. 692–697. Available at:
599 https://doi.org/10.1016/j.cub.2016.01.016.The.

600 Shee, C., Gibson, J.L. and Rosenberg, S.M. (2012) 'Two Mechanisms Produce Mutation Hotspots
601 at DNA Breaks in Escherichia coli', *Cell Reports*, 2(4), p. 714. Available at:
602 https://doi.org/10.1016/j.celrep.2012.08.033.

603 Shepherd, M.J., Horton, J.S. and Taylor, T.B. (2022) 'A near-deterministic mutational hotspot in
604 Pseudomonas fluorescens is constructed by multiple interacting genomic features', *Molecular*
605 *Biology and Evolution*, 39(6).

606 Stoltzfus, A. and Norris, R.W. (2016) 'On the Causes of Evolutionary Transition:Transversion
607 Bias', *Molecular Biology and Evolution*, 33(3), pp. 595–602. Available at:
608 https://doi.org/10.1093/molbev/msv274.

609 Taylor, T.B. *et al.* (2015) 'Evolutionary resurrection of flagellar motility via rewiring of the
610 nitrogen regulation system', *Science*, 347(6225), pp. 1014–1017. Available at:
611 https://doi.org/10.1126/science.1259145.

612